# Evolved resistance to partial GAPDH inhibition results in loss of the Warburg effect and in a different state of glycolysis

Received for publication, August 31, 2019, and in revised form, November 10, 2019 Published, Papers in Press, November 20, 2019, DOI 10.1074/jbc.RA119.010903

**Maria V. Liberti[‡§1], Annamarie E. Allen[‡], Vijyendra Ramesh[‡], Ziwei Dai[‡], Katherine R. Singleton[‡], Zufeng Guo[¶], Jun O. Liu[¶], Kris C. Wood[‡], and Jason W. Locasale[‡]**

*From the [‡]Department of Pharmacology and Cancer Biology, Duke University, Durham, North Carolina 27710, the [§]Department of Molecular Biology and Genetics, Cornell University, Ithaca, New York 14853, and the [¶]Department of Pharmacology and Molecular Sciences, Johns Hopkins University School of Medicine, Baltimore, Maryland 21205*

Edited by Jeffrey E. Pessin

**Aerobic glycolysis or the Warburg effect (WE) is characterized by increased glucose uptake and incomplete oxidation to lactate. Although the WE is ubiquitous, its biological role remains controversial, and whether glucose metabolism is functionally different during fully oxidative glycolysis or during the WE is unknown. To investigate this question, here we evolved resistance to koningic acid (KA), a natural product that specifically inhibits glyceraldehyde-3-phosphate dehydrogenase (GAPDH), a rate-controlling glycolytic enzyme, during the WE. We found that KA-resistant cells lose the WE but continue to conduct glycolysis and surprisingly remain dependent on glucose as a carbon source and also on central carbon metabolism. Consequently, this altered state of glycolysis led to differential metabolic activity and requirements, including emergent activities in and dependences on fatty acid metabolism. These findings reveal that aerobic glycolysis is a process functionally distinct from conventional glucose metabolism and leads to distinct metabolic requirements and biological functions.**

Glycolysis, the uptake and metabolism of glucose, is a set of chemical reactions conserved to the most primitive of organisms and is fundamental to sustaining life (1). Together with the catabolism of amino acids and lipids, glycolysis is a component of central carbon metabolism. The breakdown of glucose to pyruvate allows for the generation of energy in the form of ATP and reducing equivalents. In addition, glucose can be diverted into biosynthetic pathways for anabolic metabolism and for the process of metabolizing glucose to confer signaling functionality by, for example, coupling to the generation of reactive oxygen species and the mediation of chromatin state (2).

Given the numerous biological functions that are conferred through glycolysis, it is reasonable to speculate that glucose metabolism could exist in a number of distinct states that confer different phenotypes and outputs. For example, aerobic glycolysis or the Warburg effect (WE)[2] (increased glucose uptake and incomplete oxidation to lactate in the presence of oxygen) is canonically thought to constitute a switch from fully oxidative glycolysis, the more common form of metabolism observed in differentiated cells (3, 4). This altered form of glucose metabolism has been thought to result in differential functionality in cells, including variations in anabolic metabolism.

Whereas aerobic glycolysis has been extensively studied, there are contradictions regarding the biological function that it confers in cells separate from glucose metabolism. For example, findings from recent studies have questioned whether a switch from mitochondrial metabolism does in fact occur during the WE (5), which is consistent with original observations in which mitochondria remain fully functional (6, 7). Furthermore, other work has challenged whether the WE has any specific role in anabolic metabolism (8–10). In line with this notion, studies have defined metabolic requirements of cancer to exist in two states: glycolysis-dependent or -independent (11, 12). If this is the case, then the WE would not be biologically distinct from other aspects of glucose metabolism because this would suggest that only cells utilizing the WE are dependent on glycolysis. Thus, there is a surprising lack of clarity in the current literature regarding whether the WE is a biologically defined state (13).

Metabolic control analysis has indicated that GAPDH exerts more control over glycolysis during the WE (14, 15), and thus partial inhibition of GAPDH has a large differential effect on reducing glycolysis in WE conditions (16). As a proof of concept, a natural product, koningic acid (KA), was shown to be selective for GAPDH as expression of a resistant allele of GAPDH ablates all changes in metabolism induced by the compound (16–18). The compound is also selective against the fitness of cells specifically undergoing aerobic glycolysis (16, 19). Furthermore, numerous studies have suggested that targeting of GAPDH may be beneficial (20–22), in retrospect through partial inhibition of GAPDH during aerobic glycolysis. Thus, KA is a valuable probe to study the WE and to determine

This work was supported by National Institutes of Health Grants R01CA193256 (to J. W. L.), R00CA168997 (to J. W. L.), and F99CA222986 (to M. V. L.); National Science Foundation Grant DGE-1144153 (to M. V. L.); and the Sloan Foundation (to M. V. L.). Z. G. and J. O. L. are inventors on a Johns Hopkins University patent covering E11 and its use as a glucose transporter-1 inhibitor. The content is solely the responsibility of the authors and does not necessarily represent the official views of the National Institutes of Health.

This article contains Figs. S1–S5.

[1] To whom correspondence should be addressed: Rockefeller University, 1230 York Ave., New York, NY 10065. Tel.: 212-327-7220; E-mail: mliberti@rockefeller.edu.

[2] The abbreviations used are: WE, Warburg effect; GAPDH, glyceraldehyde-3-phosphate dehydrogenase; KA, koningic acid; HRMS, high-resolution MS; TCA, tricarboxylic acid; FBS, fetal bovine serum; MTT, 3-[4,5-dimethylthiazol-2-yl]-2,5-diphenyltetrazolium; ANOVA, analysis of variance.

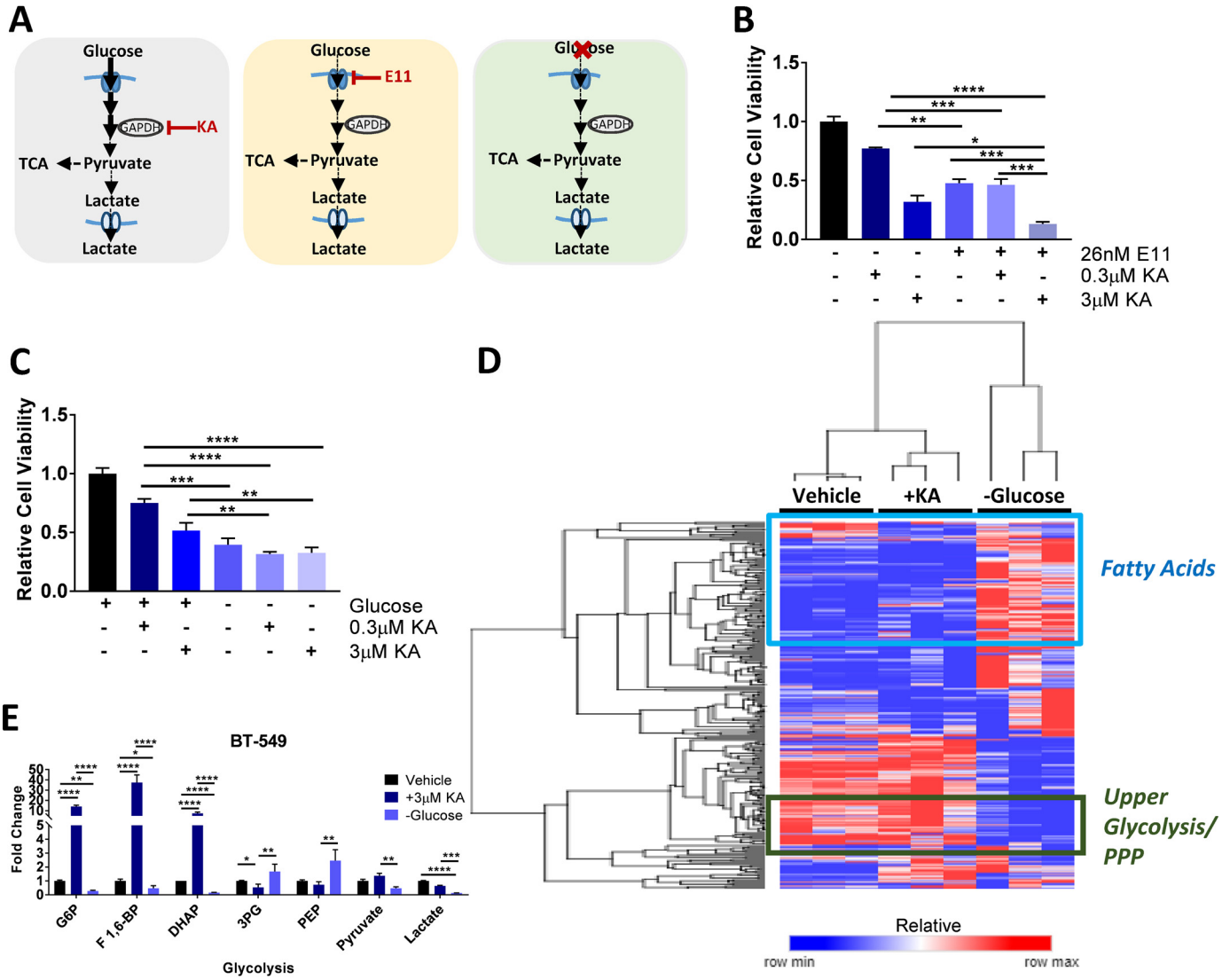


**Figure 1. GAPDH inhibition leads to different phenotypic outcomes from targeting glucose uptake.** *A, schematic* representing the comparison of KA treatment with glucose transporter-1 (GLUT-1) inhibition with E11 or deprivation of glucose from the growth medium. *B*, cell viability of BT-549 breast cancer cells treated with E11 (26 nM) with or without KA (0.3 or 3 $\mu$M) after 24 h. *, $p < 0.05$; **, $p < 0.01$; ***, $p < 0.001$; ****, $p < 0.0001$ as determined by one-way ANOVA. *C*, cell viability of BT-549 breast cancer cells cultured in complete or glucose-restricted medium and treated with or without KA (0.3 or 3 $\mu$M) after 24 h. *, $p < 0.05$; **, $p < 0.01$; ***, $p < 0.001$; ****, $p < 0.0001$ as determined by one-way ANOVA. *D*, hierarchical clustered heat map quantile-normalized of BT-549 cells with condition annotations of global metabolic responses to vehicle, 3 $\mu$M KA, or glucose-restricted conditions for 6 h with annotations of metabolic pathways. The scale represents 0 to 1 for row minimum and row maximum, respectively, after quantile normalization. *E*, BT-549 glycolysis profile for vehicle, KA, or glucose-restricted conditions for 6 h. *G6P*, glucose 6-phosphate; *F 1,6-BP*, fructose 1,6-bisphosphate; *DHAP*, dihydroxyacetone phosphate; *3PG*, 3-phosphoglycerate; *PEP*, phosphoenolpyruvate. All data are represented as mean ± S.E. (*error bars*) from $n = 3$ biological replicates. *, $p < 0.05$; **, $p < 0.01$; ***, $p < 0.001$; ****, $p < 0.0001$ as determined by two-way ANOVA unless otherwise indicated.

whether it has any distinct biological function outside of glycolysis for cellular metabolism.

In this study, we sought to address the question of whether the WE can be phenotypically defined apart from glycolysis and fully oxidative glucose metabolism. Using a series of pharmacological and metabolomic approaches, we provide evidence that glucose metabolism exists in a number of defined metabolic states. Using acquired resistance to GAPDH inhibition as a model and KA as a tool, we show that cells can simultaneously evolve loss of the WE but continue to remain dependent on glycolysis. Consequently, these cells that have a selection pressure to lose the WE display widespread changes in metabolism downstream of glycolysis changes, including a marked rewiring of fatty acid metabolism. Thus, our study provides evidence that the WE can be a biologically distinct form of glycolysis.

## Results

### *GAPDH inhibition leads to different phenotypic outcomes from targeting glucose uptake*

We first sought to determine whether disrupting GAPDH activity results in different outcomes from other perturbations to glycolysis. Because GAPDH has differential rate control in cells undergoing the WE (*i.e.* high glucose uptake and lactate secretion) (16), we used a high-WE cell line, BT-549, and compared inhibition of GAPDH with KA with inhibition of glucose uptake and deprivation of glucose from the culture medium (Fig. 1*A*). First,

we measured the $IC_{50}$ of E11, a validated, highly potent inhibitor of GLUT-1 and thus glucose uptake (23) (Fig. S1*A*). We then compared cell viability of BT-549 treated with doses of KA above and below the known $IC_{50}$ (16) and/or E11. We found that co-treatment of KA and E11 caused a greater significant decrease in cell viability than treatment with either compound alone (Fig. 1*B*). Given these data, we next carried out a dose-response assay with calculated combination indices for E11 and KA in BT-549 as well as in other cell lines that have been previously reported to undergo the WE (16) (Fig. S1, *B–F*). These results revealed synergy between KA and E11 at low to middle concentrations of KA but, more importantly, highlighted differential effects of GAPDH and GLUT-1 inhibition on cell viability.

In line with these findings, we further found significant changes between KA-treated cells and cells cultured in glucose-deprived medium (Fig. 1*C* and Fig. S1 (*G–J*)). To assess these differential effects on cells at a metabolic level, we used LC coupled to high-resolution MS (LC-HRMS)-based metabolomics, which revealed gross differences in global metabolism when comparing KA-treated BT-549 cells with glucose-deprived cells (Fig. 1*D*). An analysis of glycolysis indicated an accumulation of glycolytic intermediates upstream and depletion of those downstream of GAPDH in cells treated with KA, whereas glucose-deprived conditions revealed an overall depletion of metabolites throughout glycolysis (Fig. 1*E*). Thus, cells exhibit a differential metabolic response to GAPDH inhibition compared with other modes of glycolysis inhibition. These findings raise the possibility that cells utilize and rely on the WE differently from glycolysis, providing rationale that the WE is different from other forms of glucose metabolism.

### *Cells evolve resistance to GAPDH inhibition independent of drug metabolism*

To investigate whether glycolysis exists in different biological states from the WE, we hypothesized that cells could transition from the WE to another state of glucose metabolism when faced with a selective pressure against maintaining glycolysis in a certain state. Given that KA was previously shown to be selectively toxic to cells undergoing the WE, we suspected that it could be a useful tool to investigate this concept. We cultured BT-549 cells with incrementally increasing concentrations of KA and monitored their growth rate over a period of 20 weeks with parental cells maintained in cell culture in parallel (Fig. 2, *A* and *B*). The specific growth rate of parental cells measured after 1 week in culture was recorded as 0.0173 $h^{-1}$ and was used as the week 0 baseline measurement for beginning KA treatment for acquired resistance. Three clonal cell populations that developed resistance to KA exhibited growth rates between 0.0022 and 0.0058 $h^{-1}$. These were isolated and maintained in 3 $\mu$M KA for the remainder of the study (BT-549(R)1–3) (Fig. 2*C*). $IC_{50}$ values for KA in each of these clones were found to be greater than 200 $\mu$M compared with the parental cells that exhibited an $IC_{50}$ of ~1 $\mu$M KA (Fig. 2*D*).

For this system to be an effective model for evolving a transition out of the WE, it was necessary to first confirm that resistance to KA was not occurring due to mechanisms outside of cellular metabolism. There are several known pharmacological mechanisms that are commonly implicated in drug resistance that include alterations in drug metabolism and target disengagement (24). To test for altered drug metabolism, such as a difference in drug efflux, we used LC-HRMS to measure intracellular concentrations of KA in BT-549 sensitive and acquired resistant cells as well as in MCF-7 KA-intrinsic resistant cells (Fig. 2*E*). Intracellular concentrations of KA in BT-549 acquired resistant cells maintained in 3 $\mu$M KA remained consistent with concentrations detected in BT-549 parental and MCF-7 intrinsic resistant cells that were treated with 3 $\mu$M KA (Fig. 2*F* and Fig. S2*A*). We also found similar intracellular concentrations of KA between BT-549 parental and acquired resistant cells at different time points following culture of cells with KA (Fig. S2, *B–D*). Together, these data confirm that drug efflux is not contributing to acquired resistance to KA in these cells.

To verify that KA was still engaging its target (*i.e.* the catalytic site of GAPDH) (25, 26), we carried out a GAPDH activity assay in the presence or absence of KA and found that KA maintains target engagement through decreasing GAPDH activity in BT-549 acquired resistant cells comparable with that of BT-549 parental cells (Fig. 2*G* and Fig. S2 (*E* and *F*)) and MCF-7 cells (Fig. S2*G*). In support of these findings, we observed little difference in GAPDH protein expression between BT-549 parental and acquired resistant cells (Fig. S2*H*). We also found that acquired resistant cells can become resensitized to KA upon KA removal for 2 weeks, followed by the addition of KA again (Fig. S2*I*), further arguing against an inability to maintain target engagement. Together, these data indicate that acquired resistant cells retain normal KA drug metabolism properties with continued target engagement at the active site of GAPDH. Thus, independent of drug pharmacology, biological mechanisms related to glucose metabolism may underlie the resistance to GAPDH inhibition.

### *Acquired resistant cells lose the Warburg effect but remain dependent on glycolysis*

Using our evolved resistance model to the glycolytic enzyme GAPDH, we sought to determine whether these cells continue to undergo the WE. We treated BT-549 acquired resistant cells with KA and found that acquired resistant cells still undergo glycolysis marked by increases in fructose 1,6-bisphosphate compared with untreated BT-549 parental, which are indicative of slower rates of glycolysis (15, 27) and decreases in lactate levels compared with parental cells, suggestive of a lower WE (Fig. 3*A*). Interestingly, we also found that acquired resistant cells exhibited similar or lower levels of pentose phosphate pathway metabolites compared with parental cells (Fig. S3, *A–D*).

Because low lactate levels were detected in the acquired resistant cells compared with parental cells, we next sought to examine lactate production from glucose carbon using uniformly labeled [U-$^{13}$C]glucose in BT-549 parental and acquired resistant cells. We observed decreased lactate production in the acquired resistant cells compared with untreated parental cells at levels comparable with the lactate production observed in the parental cells treated with 3 $\mu$M KA (Fig. 3*B* and Fig. S3*E*). In addition, we measured intracellular glucose and lactate levels in

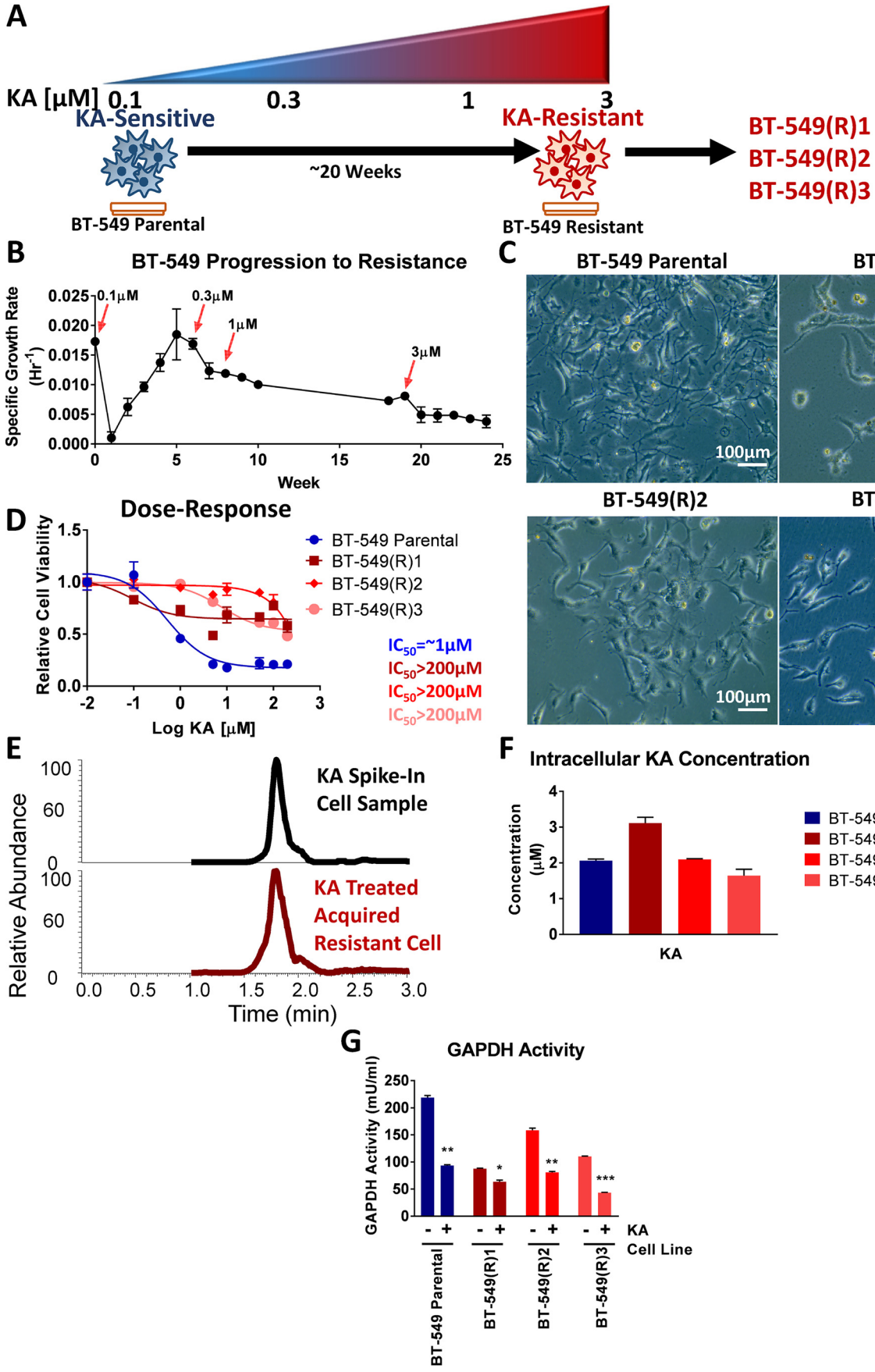

parental and acquired resistant cells (Fig. S3*F*). As expected, parental and acquired resistant cells exhibited similar intracellular glucose levels, indicative of similar glucose uptake. Parental and acquired resistant cells had similar intracellular lactate levels, which we reasoned was likely due to the majority of lactate produced by cells being immediately secreted out of cells and into the environment (4, 13). Indeed, upon measuring excreted lactate from cells in spent medium from 0 to 6 h, we found significantly less excreted lactate from BT-549 acquired resistant cells compared with parental cells treated with either vehicle or KA, with a similar finding after 24 h (Fig. 3 (*C* and *D*) and Fig. S3*G*). In addition, the decreases in lactate levels were not immediately reversible upon removal of KA (Fig. S3*H*). Quantitative measurements of the WE via relative lactate flux calculations revealed lower lactate flux (*i.e.* low WE) in acquired resistant cells compared with parental cells, with a lactate flux value comparable with the low glycolytic cell line, MCF-7 (Fig. S3*I*). Together, these data indicate that acquired resistant cells evolved a loss of the WE.

Because acquired resistant cells no longer undergo the WE, we asked whether they remained dependent on glucose uptake and depend on glycolysis for survival, because previous studies have indicated that cells are either glycolysis-dependent or -independent (11, 12). We reasoned that if these cells do continue to rely on glycolysis, which would be different from WE or non-WE cells, then another glycolytic state could have emerged. We treated the acquired resistant cells with E11 and/or KA and determined cell viability. Whereas these cells remained resistant to KA as expected, we surprisingly observed differences in sensitivity upon treatment with E11 in combination with KA (Fig. 3*E*). To further investigate this differential dependence on glycolysis, we studied the response to glucose deprivation. After 24 h of culture in glucose-deprived growth medium and KA, we found that the viability of BT-549 acquired resistant cells decreased compared with cells cultured in full growth medium and maintained in KA (Fig. 3*F*). In addition, metabolite profiling of BT-549 acquired resistant cells in glucose-deprived growth medium compared with those maintained in 3 $\mu$M KA revealed global differences in overall metabolic levels (Fig. 3*G*). Together, these data indicate that BT-549 acquired resistant cells no longer exhibit or require the WE but remain dependent on glycolysis for survival.

Interestingly, we further found that acquired resistant cells displayed decreased fraction labeling and carbon contribution from glucose through glycolysis, decreased fraction labeling with a small increase in carbon contribution from glucose through the pentose phosphate pathway, and decreased fraction labeling and carbon contribution through the citric acid (TCA) cycle (Fig. S3, *J–T*). Taken together, these data further clarify the existence of multiple states of glucose metabolism.

### *Changes in fatty acid metabolism emerge as a functional output of evolved resistance to KA*

Our data thus far indicate a transition from the utilization of the WE to loss of the WE in cells with acquired resistance to KA with changes in glucose metabolism. To understand the temporal dynamics of metabolism that result in the observed change in state of glucose metabolism, we extracted metabolites from cells at different times over the 20-week time course during progression to resistance and compared their metabolite levels with those of parental cells treated with the corresponding doses of KA (Fig. 4*A*). Metabolite profiling revealed global differences, with glycolysis most prominently affected in the parental cells and changes to fatty acid, one-carbon, and nucleotide metabolism most apparent in acquired resistant cells (Fig. 4, *B* and *C*). Over half of the common changes in each of the clones relative to the parental cells were related to fatty acid metabolism (Fig. 4*D*), including small and variably significant increases in fatty acid levels (Fig. S4, *A–C*).

Given the common changes to fatty acid metabolism and our findings that acquired resistant cells are utilizing glucose carbon differently from parental cells, we asked whether other carbon sources, such as glutamine, account for the observed differences (Fig. S4*D*). Interestingly, we found small but significant increases in the fraction labeled from glutamine through the TCA cycle, indicating that acquired resistant cells fuel their TCA cycle, at least in part, by glutamine (Fig. S4, *E–I*). Next, we analyzed whether partial increases in fatty acid levels in acquired resistant cells result from carbon contribution by glucose, glutamine, and/or palmitate and found small contributions of each of these carbon sources to representative fatty acid metabolites (Fig. S4, *J–Q*). We then asked whether removal of lipids from the extracellular environment differentially affects acquired resistant cell survival (Fig. S4*R*). We found no significant differences compared with parental cells, likely due to extracellular lipids not being a major carbon contributor in acquired resistant cells (Fig. S4, *S–U*). Together, these data demonstrate differences in fatty acid metabolism in acquired resistant cells with variable contributions from different carbon sources compared with parental cells.

To further probe the differences we observed in fatty acid metabolism, we used cerulenin, a fatty acid synthase inhibitor that inhibits fatty acid oxidation by increasing malonyl-CoA levels (28–30). We observed increased sensitivity in acquired resistant cells compared with parental cells and also found no significant change in MCF-7 cells (Fig. S5, *A–C*). Additionally, the acquired resistant cells treated with cerulenin exhibited a differential metabolic response (Fig. 5*A* and Fig. S5*D*). Next, we asked whether cerulenin differentially affected acyl-carnitine levels, signatures of fatty acid metabolism (31, 32), in BT-549

**Figure 2. Cells evolve resistance to GAPDH inhibition independent of drug metabolism.** *A, schematic* representing progression to acquired resistance model of BT-549 cells. After 20 weeks of incrementally increasing doses of KA, clonal populations of acquired resistant cells were isolated and maintained in 3 $\mu$M KA for the duration of the study. *B*, recorded growth rates of BT-549 cells during the 20-week period of progression to acquired resistance. *C*, representative images of BT-549 parental (*top left*) and three clonal acquired resistant cells (*top right*, *bottom row*). *D*, cell viability of BT-549 parental and acquired resistant cells treated with 0–200 $\mu$M KA and reported $IC_{50}$ values. *E*, mass spectra of KA in a spiked sample and KA-treated acquired resistant cells using LC-MS with a representative sample. *F*, intracellular KA concentrations from BT-549 parental and acquired resistant cells treated with 3 $\mu$M KA. *G*, relative GAPDH activity in BT-549 parental and acquired resistant cells in response to vehicle or 3 $\mu$M KA ($n = 2$). All data are represented as mean ± S.E. (*error bars*) from $n = 3$ biological replicates unless otherwise indicated. *, $p < 0.05$; **, $p < 0.01$; ***, $p < 0.001$; ****, $p < 0.0001$ as determined by multiple *t* tests.

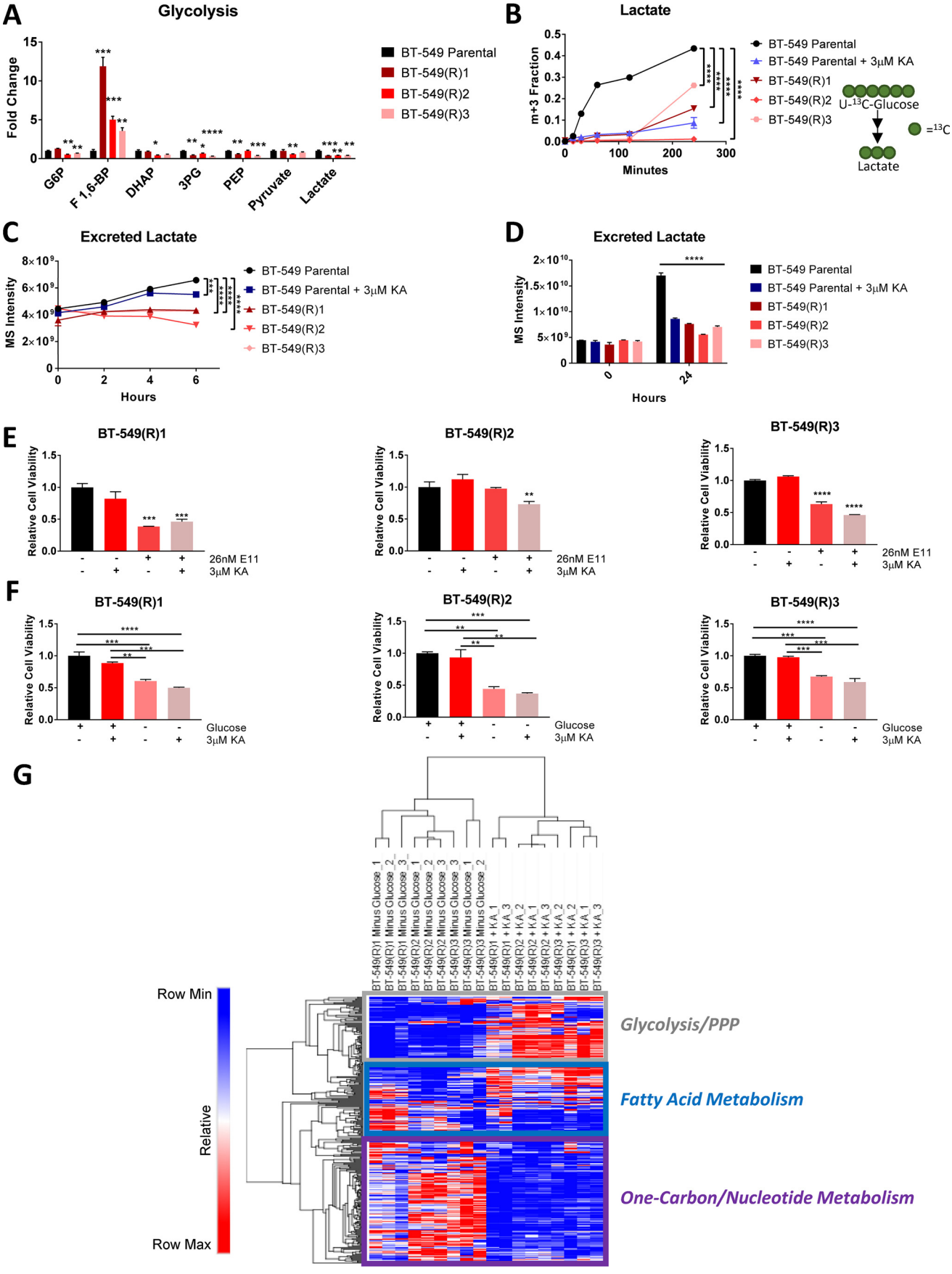

acquired resistant cells compared with BT-549 parental cells. Whereas we found that BT-549 parental cells exhibited few changes in acyl-carnitine levels upon co-treatment with KA and cerulenin, we found that when acquired resistant cells are maintained in KA, acyl-carnitines are elevated, but upon co-treatment with cerulenin, many of them significantly decrease (Fig. 5*B* and Fig. S5*E*). In corroboration with these findings, treatment with etomoxir, an inhibitor of carnitine palmitoyltransferase (CPT1), showed modest differential effects in viability of acquired resistant cells compared with parental cells, notably at 100 $\mu$M (Fig. S5*F*).

Because the biguanide metformin has been shown to decrease fatty acid and mitochondrial metabolism (33), we asked whether metformin displayed similar effects as cerulenin and etomoxir. Using the measured $IC_{50}$ of metformin in BT-549 parental cells (Fig. S5*G*), we co-treated parental and acquired resistant cells with metformin and KA, which revealed decreases in cell viability of both BT-549 parental and acquired resistant cells, albeit to a lesser extent in BT-549(R)2 cells, and no significant response in the non-glycolytic MCF-7 cells (Fig. S5, *H* and *I*). We also found that upon co-treatment with KA and metformin compared with KA alone, acyl-carnitines were to a larger extent significantly decreased in acquired resistant cells than in parental cells (Fig. 5 (*C* and *D*) and Fig. S5 (*J* and *K*)). Given the observed fatty acid metabolic phenotypes, we asked whether KA-resistant cells also depend on oxidative phosphorylation. We profiled the TCA cycle intermediates, a readout of oxidative phosphorylation, in the context of metformin inhibition in parental and KA-resistant cells (Fig. S5*L*). Upon treating parental cells with metformin in combination with KA, we observed decreases in several TCA cycle metabolites, including $\alpha$-ketoglutarate. However, whereas we found similar decreases in $\alpha$-ketoglutarate upon metformin treatment in all three resistant cell lines maintained in KA, we also observed significant or modest increases in several other TCA cycle intermediates. These results suggest that compared with parental cells, acquired resistant cells rely more on oxidative phosphorylation. Taken together, these data confirm that distinct metabolic phenotypes related to fatty acid metabolism occur downstream of the differences in glycolysis in acquired resistant cells.

## Discussion

### *Evolved resistance to KA as a model to study the Warburg effect*

Previous work has shown that GAPDH has a specific regulatory role in aerobic glycolysis (15, 16, 19, 20). Our current study extends from this understanding to show that cells that evolve resistance to a specific GAPDH inhibitor, KA, lose the WE but remain dependent on glycolysis with different metabolic outputs from cells undergoing the WE or not. In particular, we demonstrate that cells can exist in at least two separate states of glucose metabolism, including WE-dependent and glycolysis-dependent or WE-independent and glycolysis-dependent (Fig. 5*E*). Glycolysis has been thoroughly studied using models that ablate the expression of glycolytic enzymes or completely block the pathway (11, 34–36), which reduces overall or eliminates altogether the activity of glycolysis. Our model of evolved resistance to KA is useful to study glucose metabolism regulation without complete pathway inhibition. Instead, we were able to place a selection pressure against the fitness of using the WE during proliferation. Moreover, using metabolomics, we further demonstrate that the resulting pressure to lose the WE retains a requirement for glycolysis but alters several metabolic outputs in central carbon metabolism. For example, fatty acid metabolism is up-regulated and selectively required in cells. Our extensive metabolomics analyses also provide insight into enzymatic activity changes. Based on our profiling, it is worth noting that many activities in enzymes have likely changed throughout glycolysis and branching pathways. These enzyme activities, as well as the availability of different nutrients and metabolites, may also contribute to the observed fluxes through glycolysis and other biosynthetic pathways that are dependent on glycolytic metabolites. Furthermore, we could capture the temporal dynamics of metabolic alterations from early to late time points of this evolution, which also may depend on factors such as nutrient availability and enzyme activities. In physiology, such as within a tumor microenvironment, it is likely that this range of metabolic plasticity allows for rapid adaptation to a dynamic environment. A genome-wide study could be considered for future studies to complement changes observed in the metabolic network.

### *Glucose metabolism exists in distinct phenotypically distinct states*

We were able to study glycolysis under different configurations of metabolic activity as cells transition from the WE to another glycolytic state. We provide clear evidence for a distinction between the WE and glucose metabolism. Interestingly, previous literature and related drug development efforts have worked under the model that glycolysis functions as a binary switch (*i.e.* glucose-dependent or -independent) (11, 12). In these cases, glucose dependence is identical to aerobic glycolysis. Our findings show that although KA-resistant cells no longer undergo the WE, they undergo glycolysis with less lactate production and remain dependent on glucose uptake.

**Figure 3. Acquired resistant cells lose the Warburg effect but remain dependent on glycolysis.** *A*, glycolytic metabolite levels measured after 6 h. All glycolysis metabolite levels measured from parental cells were normalized to 1. All glycolysis metabolite levels measured from acquired resistant cells are normalized to parental cell levels. *, $p < 0.05$; **, $p < 0.01$; ***, $p < 0.001$; ****, $p < 0.0001$ as determined by multiple *t* tests. *B*, [$^{13}$C]lactate from [U-$^{13}$C]glucose in BT-549 parental treated with vehicle or 3 $\mu$M KA and acquired resistant cells for 0–4 h. *C*, excreted lactate detected in medium from 0 to 6 h. *D*, excreted lactate detected in medium after 24 h. *E*, cell viability of BT-549 acquired resistant cancer cells treated with E11 (26 nM) with or without KA (3 $\mu$M) after 24 h. *, $p < 0.05$; **, $p < 0.01$; ***, $p < 0.001$; ****, $p < 0.0001$ as determined by one-way ANOVA. *F*, cell viability of BT-549 acquired resistant cancer cells cultured in complete or glucose restricted medium and treated with or without KA (3 $\mu$M) after 24 h. *, $p < 0.05$; **, $p < 0.01$; ***, $p < 0.001$; ****, $p < 0.0001$ as determined by one-way ANOVA. *G*, hierarchical clustered heat map quantile-normalized of BT-549 cells with condition annotations of global metabolic responses to vehicle, 3 $\mu$M KA, or glucose-restricted conditions for 6 h with annotations of metabolic pathways. The scale represents 0 to 1 for row minimum and row maximum, respectively, after quantile normalization. *G6P*, glucose 6-phosphate; *F 1,6-BP*, fructose 1,6-bisphosphate; *DHAP*, dihydroxyacetone phosphate; *3PG*, 3-phosphoglycerate; *PEP*, phosphoenolpyruvate. All data are represented as mean ± S.E. (*error bars*) from $n = 3$ biological replicates. *, $p < 0.05$; **, $p < 0.01$; ***, $p < 0.001$; ****, $p < 0.0001$ as determined by two-way ANOVA unless otherwise indicated.

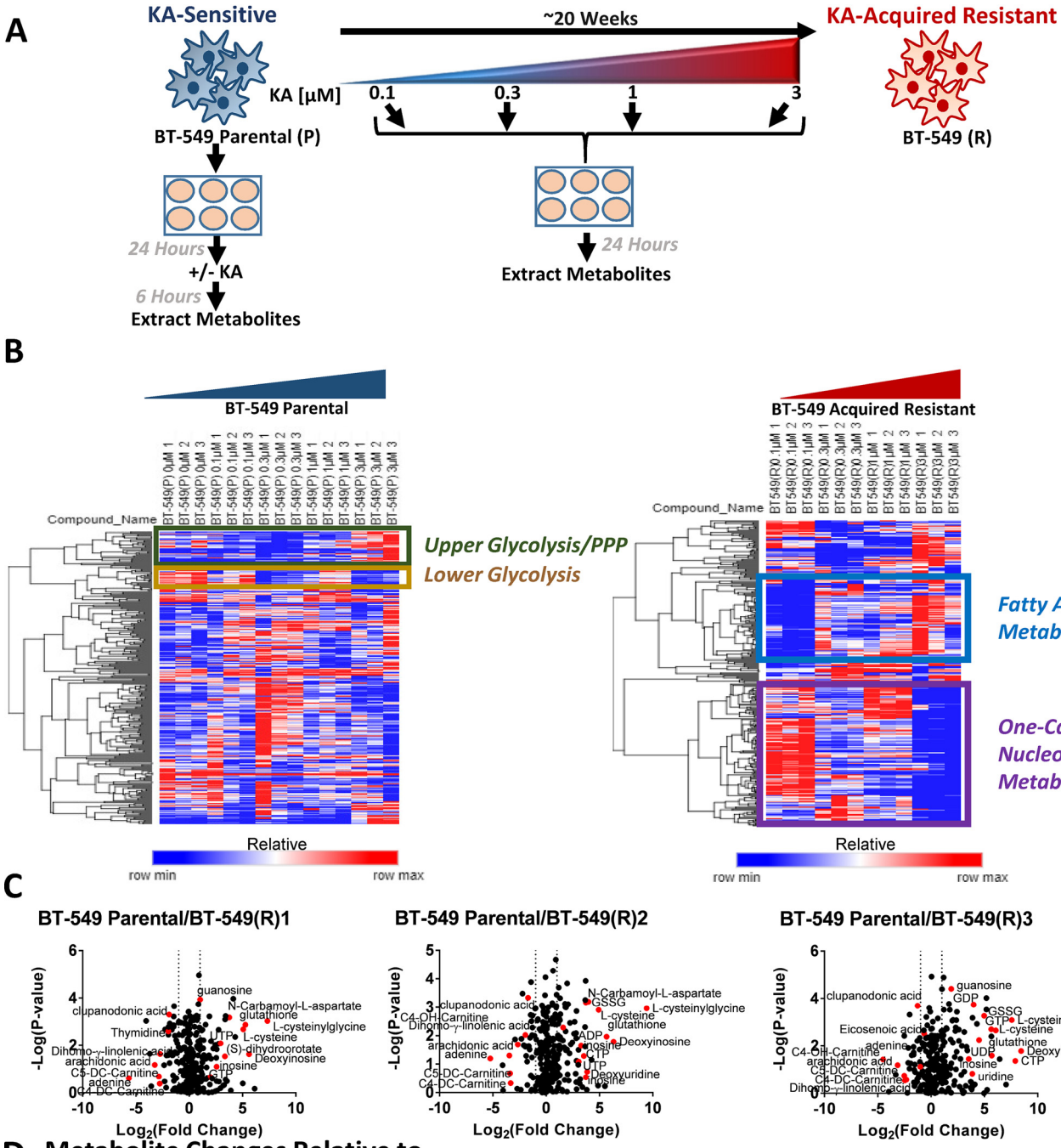


| Shared Metabolic Pathway Changes | |
|---|---|
| **Pathway** | **Number of Metabolites** |
| Fatty Acid Metabolism | 19 |
| Nucleotide Metabolism | 7 |
| Glucose Metabolism | 4 |
| Nicotinamide Metabolism | 3 |
| Others | 8 |

Whereas the difference in intracellular lactate levels between parental cells treated with KA and acquired resistant cells maintained in KA was not as dramatic as was seen with measurements of secreted lactate, the majority of lactate produced by cells is immediately secreted into the environment (4, 13), likely accounting for the larger differential found in secreted lactate. Thus, our data indicate that glucose metabolism exists functionally in a set of states, depending on selective pressures and demands for cellular survival. By evolving resistance to GAPDH inhibition with KA, we show that WE-undergoing cells that lose aerobic glycolysis do not simply switch to increased oxidative phosphorylation but maintain glucose metabolism in a separate biological state with separate metabolic outputs.

### *The biology of and targeting of the Warburg effect*

Although aerobic glycolysis has been extensively studied over the years, whether the WE has a function aside from glycolysis has been questioned (8, 37). Our findings provide evidence for the WE existing as a biologically functional state of glucose metabolism. From a therapeutic perspective, elucidating the WE as a distinct phenomenon from glucose metabolism provides a rationale for continued efforts to target the WE while keeping all other forms of glycolysis intact. Such efforts are under way, including various studies particularly focusing on the targeting of GAPDH (19–21). The practicability of targeting GAPDH therapeutically likely results from the ability to target its activity. GAPDH is a highly abundant protein and is the most abundant protein in glycolysis (38). In addition, previous reports record that most cancer types exhibit moderate GAPDH protein staining relative to normal tissues (39, 40), indicating that GAPDH levels between normal and cancer cells are not considered to be different from each other. Thus, cells undergoing the WE exhibit higher GAPDH activity irrespective of protein level, which has been shown to be associated with increased sensitivity to GAPDH inhibition (15, 16). Additional studies also indicate the feasibility and tolerability of targeting GAPDH therapeutically in disease contexts (16, 19).

This current study now provides evidence for a proof-of-principle concept in which acquired resistance to a potential cancer therapy can be encoded in the metabolic activity of the metabolic network controlled by the therapeutic target (*i.e.* GAPDH). This study further shows that acquired resistance from inhibition of the WE can result in an altered glycolytic state whereby cells still remain dependent on glucose carbon for fueling their metabolic demands. These findings provide clinical relevance and systematic strategies for therapeutically targeting pathways in the central carbon network upon acquired resistance to inhibiting the WE, such as fatty acid metabolism. Notably, the WE and high rates of glycolysis have been shown to complement fatty acid metabolism in a tumor setting (41). One potential reason for this could be due to glucose-derived pyruvate incorporation into the TCA cycle, which would fuel fatty acid metabolism and synthesis.

The implications of our findings could extend to effective strategies in the tumor microenvironment as well, especially given the efficacy of KA on immune cell populations that rely on glycolysis for activation. Beyond the clinical implications of understanding acquired resistance to the WE, we now provide insight onto how cells can metabolically evolve resistance to a metabolic inhibitor over time. This is an important concept that can apply to other clinically relevant targeted metabolic therapies, such as 5-fluorouracil or gemcitabine, both of which have exhibited challenges clinically due to resistance. Although this study by itself does not resolve whether the WE is in fact driving cancer or whether it is a metabolic consequence of cancer progression, it does confirm that the WE is a real biological phenomenon with different biological and metabolic properties.

## Experimental procedures

### *Cell culture*

BT-549 and MCF-7 cells were cultured in full medium containing RPMI 1640 (Gibco), 10% heat-inactivated fetal bovine serum (FBS), 100 units/ml penicillin, and 100 $\mu$g/ml streptomycin. BT-549 and MCF-7 cells were obtained from the American Tissue Culture Collection (ATCC). KA-resistant BT-549 cells were cultured and maintained in full medium containing RPMI 1640, 10% heat-inactivated FBS, 100 units/ml penicillin, 100 $\mu$g/ml streptomycin, and 3 $\mu$M KA (isolated in-house) (16). Cells were cultured in a 37 °C, 5% $CO_2$ atmosphere.

### *Time to progression to resistance assay*

Cells were allowed to progress to resistance as described previously (42). To allow cells to acquire resistance to KA, BT-549 breast cancer cells were first seeded in triplicate in 15-cm plates at $3 \times 10^6$ cells/plate in normal medium. After 24 h, the normal growth medium was replaced with fresh medium at the indicated KA treatment. After 7 days, cells were lifted with 0.25% trypsin (Cellgro) and counted using a Moxi Z mini automated cell counter. All cells up to $1 \times 10^6$ cells were centrifuged at 1,500 rpm for 3 min, resuspended in 10 ml of medium, and plated into a 15-cm plate with fresh treatment. For each measurement, once cell number reached $3 \times 10^6$ cells 2 weeks in a

**Figure 4. Changes in fatty acid metabolism emerge as a functional output of evolved resistance to KA.** *A*, *schematic* of experimental setup for metabolomics during evolution to acquired resistance to KA. Metabolites from parental cells were extracted after 6 h of treatment with 0–3 $\mu$M KA. Metabolites from KA-acquired resistant cells were extracted over the 20-week progression to resistance period upon resistance to the depicted doses. *B*, hierarchical clustered heat maps quantile-normalized. Shown is a heat map depicting detected metabolites from parental cells treated with 0–3 $\mu$M KA for 6 h (*left*) and a heat map depicting detected metabolites as cells acquire resistance to 0–3 $\mu$M KA over 20 weeks (*right*). Heat maps show annotations of metabolite pathways. The scale represents 0 to 1 for row minimum and row maximum, respectively, after quantile normalization. *C*, volcano plots showing metabolite profiles of BT-549 acquired resistant cells maintained in 3 $\mu$M KA compared with BT-549 parental cells treated with vehicle. Shown is $\log_2$ -fold change *versus* $-\log_{10} p$ value. *Dotted lines* along the *x* axis represent $\pm\log_2(1)$ -fold change, and the *dotted line* along the *y* axis represents $-\log_{10}(0.05)$. Metabolites $\pm \log_2(1)$ -fold change are shown as *red points* with metabolite names denoted. All other metabolites are shown as *black points*. *D*, Venn diagram indicating the overlap of metabolic changes among KA-resistant clones based on average $\pm\log_2(1)$ -fold changes compared with BT-549 parental cells treated with vehicle. *G6P*, glucose 6-phosphate; *F 1,6-BP*, fructose 1,6-bisphosphate; *DHAP*, dihydroxyacetone phosphate; *3PG*, 3-phosphoglycerate; *PEP*, phosphoenolpyruvate. All data are represented as mean ± S.E. from $n = 3$ biological replicates. *, $p < 0.05$; **, $p < 0.01$; ***, $p < 0.001$; ****, $p < 0.0001$ as determined by two-way ANOVA.

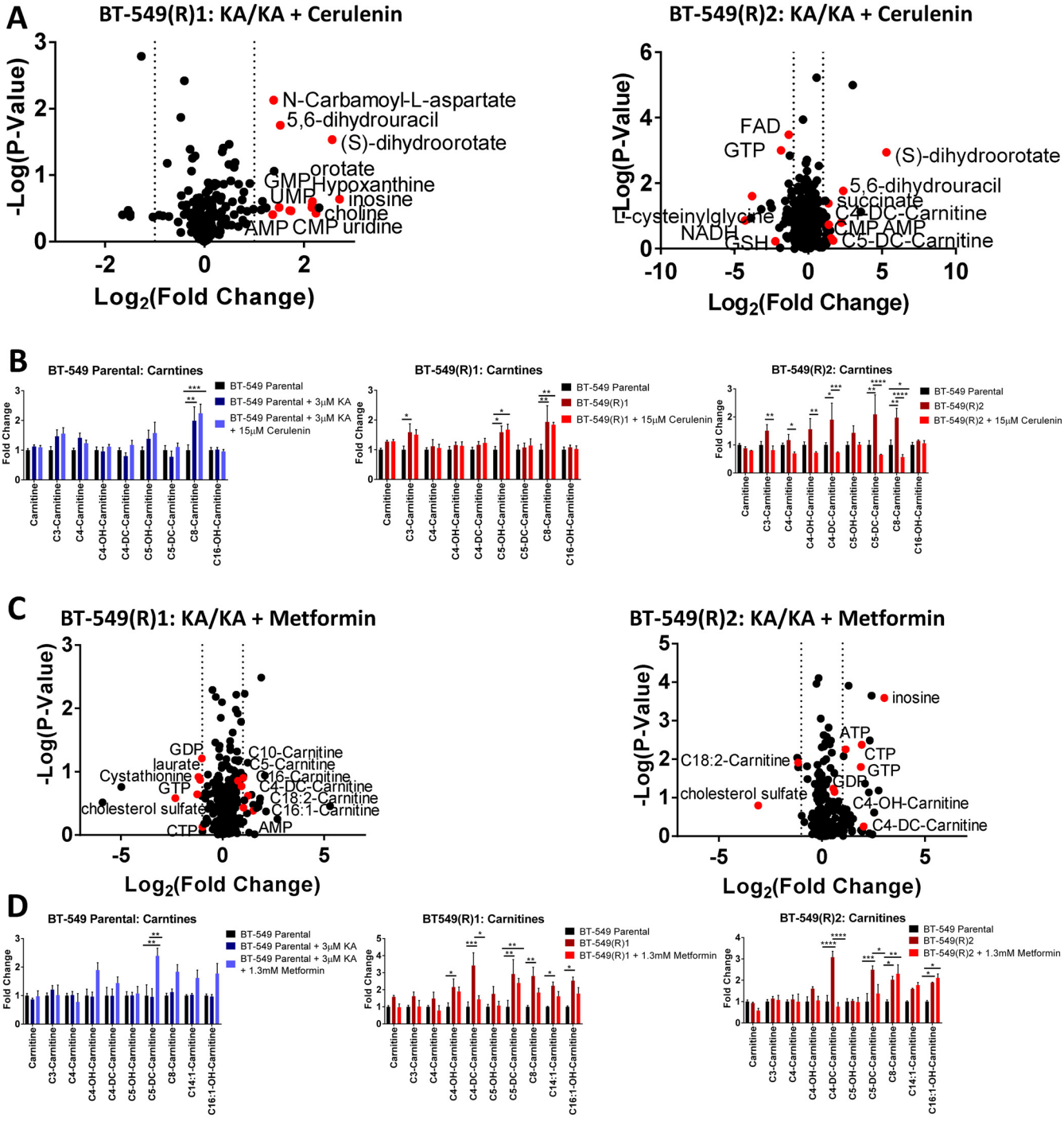

row, the dose was increased as indicated. This procedure was repeated weekly for 20 weeks. Weekly growth rates ($\mu$) were calculated from the number of cells plated the previous week ($N_0$) and the number of cells counted in the current week ($N$) according to the formula,

$$\ln N = \ln N_0 + \mu t \quad \text{(Eq. 1)}$$

where $t$ is elapsed time in hours. These growth rates were then used to project total cell number as if no cells had been discarded.

### Cell viability assays

For all cell lines, $5 \times 10^4$ cells/well were seeded in triplicate in a 96-well plate and allowed to adhere for 24 h. The following day, vehicle or treatment was added to each well at the respective concentrations. After 24 h, the medium was aspirated and replaced with 100 $\mu$l of phenol red–free RPMI 1640, and 12 mM 3-[4,5-dimethylthiazol-2-yl]-2,5-diphenyltetrazolium (MTT) (Thermo Fisher Scientific, #M6494) was added to the cells. After 4 h, the medium containing MTT was aspirated, and 50 $\mu$l of DMSO was added to dissolve the formazan and read at 540 nm.

### Drug treatments

For all cell lines, $IC_{50}$ values of KA were measured by seeding $5 \times 10^4$ cells/well in triplicate in a 96-well plate and allowed to adhere for 24 h. The following day, medium was changed, and concentrations of either vehicle ($H_2O$ or DMSO), KA, E11 (23), cerulenin (Sigma-Aldrich, #C2389), metformin (Santa Cruz Biotechnology, #202000A), or etomoxir (Sigma-Aldrich, #E1905) were added. After 24 h, cell viability assays were carried out using MTT as described previously.

### Nutrient restriction in medium

For all cell lines, $5 \times 10^4$ cells/well were seeded in triplicate with complete RPMI 1640 medium in 96-well plates and allowed to adhere for 24 h. On the following day, the respective treatment medium was added in the absence or presence of KA at the indicated treatments. MTT assays were carried out as described previously. Treatment medium used was as follows: minus glucose (−Glucose): RPMI 1640 with glutamine lacking glucose containing 10% dialyzed FBS (Life Technologies), 100 units/ml penicillin, and 100 $\mu$g/ml streptomycin; delipidated serum (D-FBS): RPMI 1640 with glutamine containing 10% delipidated FBS (Thermo Fisher Scientific, #A3382101), 100 units/ml penicillin, and 100 $\mu$g/ml streptomycin. Cells were grown at 37 °C with 5% $CO_2$.

### Synergism experiments

BT-549, SK-MEL-28, SK-MEL-5, and NCI-H522 cell lines were seeded at $5 \times 10^4$ cells/well in 96-well plates and allowed to adhere for 24 h prior to treatment. After, 0, 0.5, 1, 5, and 10 $\mu$M KA were used as single concentrations or in combination with 0, 10, 100, 500, and 1,000 nM E11 or in combination with 0, 0.5, 1, 5, and 11 mM glucose. After 24 h, dose-response curves were generated using MTT reagent as described above. Then cell viability values and concentrations were inputted into CompuSyn 1.0 software, and combination indices were calculated by the software to determine synergism, additivity, or antagonism.

### Resensitization of BT-549 acquired resistant cells to KA

KA was removed from BT-549 acquired resistant cells for 3 passages (~2 weeks) (BT-549(R)1–3$^{-KA,p.3}$). After, parental cells, acquired resistant cells maintained in 3 $\mu$M KA, and BT-549(R)1–3$^{-KA,p.3}$ cells were treated with vehicle, 0.5 $\mu$M, or 3 $\mu$M KA for 24 h followed by measurement of cell viability with MTT reagent.

### GAPDH activity assay

A GAPDH activity assay kit (BioVision, #K680) was used. All cells were seeded at $1 \times 10^6$ cells/10-cm plate with either vehicle or KA. After 24 h, cells were lysed, an NADH standard curve was made, and cells were measured at 450 nm in kinetic mode for 60 min at 37 °C according to the manufacturer's instructions.

### Microscopy

Cells were seeded at a density of $5 \times 10^3$ cells/well in 6-well plates and allowed to adhere for 24 h prior to treatment. After 48 h, images were captured using a Leica DM IL LED microscope equipped with a Leica MC170HD camera at ×10 objective using LAS EZ software (Leica). *Scale bars* represent 100 $\mu$m.

### Stable isotope labeling

Cells were seeded at $3 \times 10^5$ cells/well in a 6-well plate and allowed to adhere for 24 h. For [U-$^{13}$C]glucose isotopic labeling, cells were treated with either vehicle or KA for 6 h and then replaced with RPMI 1640 medium containing 11 mM [U-$^{13}$C] glucose (Cambridge Isotope Laboratories, #CLM-1396) and vehicle or KA for 0–4 h or for 24 h. Metabolites were then extracted. For [U-$^{13}$C]glutamine isotopic labeling, cells were treated with either vehicle or KA for 6 h and then replaced with RPMI 1640 medium containing 10% dialyzed FBS, 2 mM [U-$^{13}$C]glutamine (Cambridge Isotope Laboratories, #CLM-1822), and vehicle or KA for 24 h. Metabolites were then

**Figure 5. Changes in fatty acid metabolism occur downstream of differences in glycolysis in acquired resistance to KA.** *A*, volcano plots showing metabolite profiles of BT-549 acquired resistant (R)1 and (R)2 cells maintained in KA (3 $\mu$M) with or without cerulenin (15 $\mu$M). $Log_2$ -fold change *versus* $-log_{10}$ *p* value. *Dotted lines* along the *x* axis represent $\pm log_2(1)$ -fold change, and the *dotted line* along the *y* axis represents $-log_{10}(0.05)$. Metabolites $\pm$ $log_2(1)$ -fold change are shown as *red points* with metabolite names denoted. All other metabolites are *black points*. *B*, acyl-carnitine levels in BT-549 parental and acquired resistant cells maintained in KA (3 $\mu$M) and treated with or without cerulenin (15 $\mu$M) for 6 h. *C*, volcano plots showing metabolic profiles of BT-549 acquired resistant (R)1 and (R)2 cells maintained in KA (3 $\mu$M) with or without metformin (1.3 mM) as in *A*. *D*, acyl-carnitine levels in BT-549 parental and acquired resistant cells maintained in KA (3 $\mu$M) and treated with or without metformin (1.3 mM) for 6 h. *E*, *schematic* representing different phenotypically defined glucose metabolism states. *SAH*, *S*-adenosyl-L-homocysteine. All data are represented as mean ± S.E. (*error bars*) from $n = 3$ biological replicates. *, $p < 0.05$; **, $p < 0.01$; ***, $p < 0.001$; ****, $p < 0.0001$ as determined by two-way ANOVA.

extracted. For [U-$^{13}$C]palmitate isotopic labeling, cells were treated with vehicle or KA for 6 h and then replaced with RPMI 1640 medium containing 10% dialyzed FBS, 100 $\mu$M [U-$^{13}$C]palmitate (Cambridge Isotope Laboratories, #CLM-409), and vehicle or KA for 24 h. Metabolites were then extracted.

### Intracellular metabolite measurements

Cells were seeded at $3 \times 10^5$ cells/well in a 6-well plate and allowed to adhere for 24 h. After, cells were treated with vehicle or KA for 6 h and then washed twice with 0.9% NaCl. Metabolites were then extracted.

### Extracellular metabolite excretion measurements

Cells were seeded at $3 \times 10^5$ cells/well in a 6-well plate and allowed to adhere for 24 h. After, cells were treated with vehicle or KA, and 15 $\mu$l of medium was collected from 0 to 4 h and 24 h. Metabolites were then extracted.

### Metabolite extraction

Metabolite extraction and subsequent LC-HRMS for polar metabolites of each cell line were carried out using a Q Exactive Plus mass spectrometer as described previously (43, 44). For culture from adherent cell lines, medium was quickly aspirated. Next, 1 ml of extraction solvent (80% methanol/water) cooled to −80 °C overnight was added immediately to each well, and the plates were then transferred to −80 °C for 15 min. After, the plates were removed, and cells were scraped into the extraction solvent on dry ice. For medium extractions, 15 $\mu$l of medium was collected at 0–24 h. Next, 15 $\mu$l of extraction solvent (80% methanol/water) (Optima LC-MS grade, Fisher; methanol, #A456; water, #W6) was added to the medium. For absolute quantification of KA in cells, medium was quickly aspirated, and cells were washed twice with 0.9% NaCl following extraction for culture from adherent cells. 0.7 $\mu$M KA in water was added into extraction solvent before centrifugation. For absolute quantification of KA at 2, 6, and 24 h, cells were washed twice with 0.9% NaCl, and a standard curve of KA was applied with concentrations from 0 to 25 $\mu$M KA added into methanol solvent of untreated BT-549 cells before centrifugation. All metabolite extractions were centrifuged at 20,000 × *g* at 4 °C for 10 min. Finally, the solvent in each sample was evaporated using a speed vacuum for metabolite analysis. For polar metabolite analysis, the cell metabolite extract was first dissolved in 15 $\mu$l of water, followed by dilution with 15 $\mu$l of methanol/acetonitrile (1:1, v/v) (Optima LC-MS grade, Fisher; methanol, #A456; acetonitrile, #A955). Samples were centrifuged at 20,000 × *g* for 10 min at 4 °C, and the supernatants were transferred to LC vials. The injection volume for polar metabolite analysis was 5 $\mu$l.

### Liquid chromatography

An XBridge amide column (100 × 2.1-mm inner diameter, 3.5 $\mu$m; Waters) was used on a Dionex (Ultimate 3000 UHPLC) for compound separation at room temperature. Mobile phase A is water with 5 mM ammonium acetate, pH 6.9, and mobile phase B is 100% acetonitrile. The gradient is linear as follows: 0 min, 85% B; 1.5 min, 85% B; 5.5 min, 35% B; 10 min, 35% B; 10.5 min, 35% B; 10.6 min, 10% B; 12.5 min, 10% B; 13.5 min, 85% B; and 20 min, 85% B. The flow rate was 0.15 ml/min from 0 to 5.5 min, 0.17 ml/min from 6.9 to 10.5 min, 0.3 ml/min from 10.6 to 17.9 min, and 0.15 ml/min from 18 to 20 min. All solvents are LC-MS grade and were purchased from Fisher.

### Mass spectrometry

The Q Exactive Plus mass spectrometer (Thermo Scientific) is equipped with a heated electrospray ionization probe, and the relevant parameters were as listed: evaporation temperature, 120 °C; sheath gas, 30; auxiliary gas, 10; sweep gas, 3; spray voltage, 3.6 kV for positive mode and 2.5 kV for negative mode. Capillary temperature was set at 320 °C, and S lens was 55. A full scan range from 70 to 900 (*m/z*) was used. The resolution was set at 70,000. The maximum injection time was 200 ms. Automated gain control was targeted at $3 \times 10^6$ ions.

### Peak extraction and data analysis

Raw data collected from LC-Q Exactive Plus MS was processed on Sieve 2.0 (Thermo Scientific). Peak alignment and detection were performed according to the protocol described by Thermo Scientific. For a targeted metabolite analysis, the method "peak alignment and frame extraction" was applied. An input file of theoretical *m*/*z* and detected retention time of 197 known metabolites was used for targeted metabolite analysis with data collected in positive mode, whereas a separate input file of 262 metabolites was used for negative mode. *m*/*z* width was set to 10 ppm. The output file including detected *m*/*z* and relative intensity in different samples was obtained after data processing. If the lowest integrated mass spectrometer signal (MS intensity) was less than 1,000 and the highest signal was less than 10,000, then this metabolite was considered below the detection limit and excluded for further data analysis. If the lowest signal was less than 1,000, but the highest signal was more than 10,000, then a value of 1,000 was imputed for the lowest signals. Mass isotopomer distributions were calculated, and samples were normalized by comparing the ratio of glucose-derived labeled metabolites to unlabeled metabolites within each sample. Quantitation and statistics were calculated using Microsoft Excel and GraphPad Prism 7.0.

### Analysis of metabolomics data

GENE-E and Morpheus software were used for hierarchical clustering and heat map generation (Broad Institute, https://software.broadinstitute.org/GENE-E/index.html).[3] For hierarchical clustering, Spearman correlation parameters were implemented for row and column parameters, with the exception of BT-549 parental and acquired resistant drug response data, in which hierarchical clustering for row parameters only was used. Quantile normalization was used to normalize the data, represented by color scales.

### Lactate flux calculations

The time-dependent lactate-labeling pattern was modeled as with the equation,

[3] Please note that the JBC is not responsible for the long-term archiving and maintenance of this site or any other third party hosted site.

$$\frac{[X^*]}{X^T} = 1 - e^{-\frac{f_X}{X^T}t} \quad \text{(Eq. 2)}$$

In which $[X^*]$ is the concentration of labeled lactate, $X^T$ is the total concentration (both labeled and unlabeled) of lactate, and $f_X$ is the lactate production flux. This model was fit to lactate mass isotopomer distributions using the fit() function in MATLAB to determine relative lactate production fluxes. Relative lactate pool sizes were estimated from MS signal intensities.

### Quantification and statistical analysis

Unless otherwise noted, all *error bars* represent reported ± S.E. with $n = 3$ independent biological measurements, and statistical tests resulting in $p$ value computations were computed using two-tailed Student's $t$ test, multiple $t$ tests, one-way ANOVA, or two-way ANOVA of log-transformed data followed by Tukey's multiple comparisons. All statistics were computed using GraphPad Prism 7 (GraphPad Software, Inc.).

*Author contributions*—M. V. L. and J. W. L. conceptualization; M. V. L., A. E. A., V. R., and Z. D. data curation; M. V. L., V. R., Z. D., K. R. S., Z. G., J. O. L., K. C. W., and J. W. L. formal analysis; M. V. L. and J. W. L. supervision; M. V. L. and J. W. L. validation; M. V. L., K. R. S., and J. W. L. investigation; M. V. L., Z. D., K. R. S., K. C. W., and J. W. L. methodology; M. V. L. and J. W. L. writing-original draft; M. V. L. project administration; M. V. L., A. E. A., J. O. L., K. C. W., and J. W. L. writing-review and editing; Z. G. and J. O. L. resources.

*Acknowledgments—We thank the members of the Locasale laboratory for comments and advice.*

### References


1. Bar-Even, A., Flamholz, A., Noor, E., and Milo, R. (2012) Rethinking glycolysis: on the biochemical logic of metabolic pathways. *Nat. Chem. Biol.* **8,** 509–517 CrossRef Medline
2. Chandel, N. S. (2015) *Navigating Metabolism*, Cold Spring Laboratory Press, New York
3. DeRisi, J. L., Iyer, V. R., and Brown, P. O. (1997) Exploring the metabolic and genetic control of gene expression on a genomic scale. *Science* **278,** 680–686 CrossRef Medline
4. Vander Heiden, M. G., Cantley, L. C., and Thompson, C. B. (2009) Understanding the Warburg effect: the metabolic requirements of cell proliferation. *Science* **324,** 1029–1033 CrossRef Medline
5. Sellers, K., Fox, M. P., Bousamra, M., 2nd, Slone, S. P., Higashi, R. M., Miller, D. M., Wang, Y., Yan, J., Yuneva, M. O., Deshpande, R., Lane, A. N., and Fan, T. W. (2015) Pyruvate carboxylase is critical for non–small-cell lung cancer proliferation. *J. Clin. Invest.* **125,** 687–698 CrossRef Medline
6. Warburg, O., Wind, F., and Negelein, E. (1927) The metabolism of tumors in the body. *J. Gen. Physiol.* **8,** 519–530 CrossRef Medline
7. Crabtree, H. G. (1929) Observations on the carbohydrate metabolism of tumours. *Biochem. J.* **23,** 536–545 CrossRef Medline
8. Hosios, A. M., Hecht, V. C., Danai, L. V., Johnson, M. O., Rathmell, J. C., Steinhauser, M. L., Manalis, S. R., and Vander Heiden, M. G. (2016) Amino acids rather than glucose account for the majority of cell mass in proliferating mammalian cells. *Dev. Cell* **36,** 540–549 CrossRef Medline
9. DeBerardinis, R. J., Mancuso, A., Daikhin, E., Nissim, I., Yudkoff, M., Wehrli, S., and Thompson, C. B. (2007) Beyond aerobic glycolysis: transformed cells can engage in glutamine metabolism that exceeds the requirement for protein and nucleotide synthesis. *Proc. Natl. Acad. Sci. U.S.A.* **104,** 19345–19350 CrossRef Medline
10. Hu, C.-M., Tien, S. C., Hsieh, P. K., Jeng, Y. M., Chang, M. C., Chang, Y. T., Chen, Y. J., Chen, Y. J., Lee, E. Y. P., and Lee, W. H. (2019) High glucose triggers nucleotide imbalance through *O*-GlcNAcylation of key enzymes and induces KRAS mutation in pancreatic cells. *Cell Metab.* **29,** 1334–1349.e10 CrossRef Medline
11. Pusapati, R. V., Daemen, A., Wilson, C., Sandoval, W., Gao, M., Haley, B., Baudy, A. R., Hatzivassiliou, G., Evangelista, M., and Settleman, J. (2016) mTORC1-dependent metabolic reprogramming underlies escape from Glycolysis addiction in cancer cells. *Cancer Cell* **29,** 548–562 CrossRef Medline
12. Boudreau, A., Purkey, H. E., Hitz, A., Robarge, K., Peterson, D., Labadie, S., Kwong, M., Hong, R., Gao, M., Del Nagro, C., Pusapati, R., Ma, S., Salphati, L., Pang, J., Zhou, A., *et al.* (2016) Metabolic plasticity underpins innate and acquired resistance to LDHA inhibition. *Nat. Chem. Biol.* **12,** 779–786 CrossRef Medline
13. Liberti, M. V., and Locasale, J. W. (2016) The Warburg effect: how does it benefit cancer cells? *Trends Biochem. Sci.* **41,** 211–218 CrossRef Medline
14. Bakker, B. M., Westerhoff, H. V., Opperdoes, F. R., and Michels, P. A. (2000) Metabolic control analysis of glycolysis in trypanosomes as an approach to improve selectivity and effectiveness of drugs. *Mol. Biochem. Parasitol.* **106,** 1–10 CrossRef Medline
15. Shestov, A. A., Liu, X., Ser, Z., Cluntun, A. A., Hung, Y. P., Huang, L., Kim, D., Le, A., Yellen, G., Albeck, J. G., and Locasale, J. W. (2014) Quantitative determinants of aerobic glycolysis identify flux through the enzyme GAPDH as a limiting step. *Elife* **3,** e03342 CrossRef Medline
16. Liberti, M. V., Dai, Z., Wardell, S. E., Baccile, J. A., Liu, X., Gao, X., Baldi, R., Mehrmohamadi, M., Johnson, M. O., Madhukar, N. S., Shestov, A. A., Chio, I. I. C., Elemento, O., Rathmell, J. C., Schroeder, F. C., McDonnell, D. P., and Locasale, J. W. (2017) A predictive model for selective targeting of the Warburg effect through GAPDH inhibition with a natural product. *Cell Metab.* **26,** 648–659.e8 CrossRef Medline
17. Watanabe, H., Hasumi, K., Fukushima, Y., Sakai, K., and Endo, A. (1993) Cloning of two isozymes of *Trichoderma koningii* glyceraldehyde-3-phosphate dehydrogenase with different sensitivity to koningic acid. *Biochim. Biophys. Acta* **1172,** 43–48 CrossRef Medline
18. Kumagai, S., Narasaki, R., and Hasumi, K. (2008) Glucose-dependent active ATP depletion by koningic acid kills high-glycolytic cells. *Biochem. Biophys. Res. Commun.* **365,** 362–368 CrossRef Medline
19. Kornberg, M. D., Bhargava, P., Kim, P. M., Putluri, V., Snowman, A. M., Putluri, N., Calabresi, P. A., and Snyder, S. H. (2018) Dimethyl fumarate targets GAPDH and aerobic glycolysis to modulate immunity. *Science* **360,** 449–453 CrossRef Medline
20. Yun, J., Mullarky, E., Lu, C., Bosch, K. N., Kavalier, A., Rivera, K., Roper, J., Chio, I. I., Giannopoulou, E. G., Rago, C., Muley, A., Asara, J. M., Paik, J., Elemento, O., Chen, Z., *et al.* (2015) Vitamin C selectively kills KRAS and BRAF mutant colorectal cancer cells by targeting GAPDH. *Science* **350,** 1391–1396 CrossRef Medline
21. Louie, S. M., Grossman, E. A., Crawford, L. A., Ding, L., Camarda, R., Huffman, T. R., Miyamoto, D. K., Goga, A., Weerapana, E., and Nomura, D. K. (2016) GSTP1 is a driver of triple-negative breast cancer cell metabolism and pathogenicity. *Cell Chem. Biol.* **23,** 567–578 CrossRef Medline
22. Ganapathy-Kanniappan, S., Geschwind, J. F., Kunjithapatham, R., Buijs, M., Vossen, J. A., Tchernyshyov, I., Cole, R. N., Syed, L. H., Rao, P. P., Ota, S., and Vali, M. (2009) Glyceraldehyde-3-phosphate dehydrogenase (GAPDH) is pyruvylated during 3-bromopyruvate mediated cancer cell death. *Anticancer Res.* **29,** 4909–4918 Medline
23. Liu, J., Jingxin, W., and Guo, Z. (August 10, 2017) Rapaglutins, novel inhibitors of glut and use thereof, International Patent WO2017136731A1
24. Holohan, C., Van Schaeybroeck, S., Longley, D. B., and Johnston, P. G. (2013) Cancer drug resistance: an evolving paradigm. *Nat. Rev. Cancer* **13,** 714–726 CrossRef Medline
25. Endo, A., Hasumi, K., Sakai, K., and Kanbe, T. (1985) Specific inhibition of glyceraldehyde-3-phosphate dehydrogenase by koningic acid (heptelidic acid). *J. Antibiot.* **38,** 920–925 CrossRef Medline
26. Sakai, K., Hasumi, K., and Endo, A. (1988) Inactivation of rabbit muscle glyceraldehyde-3-phosphate dehydrogenase by koningic acid. *Biochim. Biophys. Acta* **952,** 297–303 CrossRef Medline

27. van Heerden, J. H., Wortel, M. T., Bruggeman, F. J., Heijnen, J. J., Bollen, Y. J., Planqué, R., Hulshof, J., O'Toole, T. G., Wahl, S. A., and Teusink, B. (2014) Lost in transition: start-up of glycolysis yields subpopulations of nongrowing cells *Science* **343,** 1245114 CrossRef Medline
28. Hu, Z., Cha, S. H., Chohnan, S., and Lane, M. D. (2003) Hypothalamic malonyl-CoA as a mediator of feeding behavior. *Proc. Natl. Acad. Sci. U.S.A.* **100,** 12624–12629 CrossRef Medline
29. Loftus, T. M., Jaworsky, D. E., Frehywot, G. L., Townsend, C. A., Ronnett, G. V., Lane, M. D., and Kuhajda, F. P. (2000) Reduced food intake and body weight in mice treated with fatty acid synthase inhibitors. *Science* **288,** 2379–2381 CrossRef Medline
30. Thupari, J. N., Pinn, M. L., and Kuhajda, F. P. (2001) Fatty acid synthase inhibition in human breast cancer cells leads to malonyl-CoA-induced inhibition of fatty acid oxidation and cytotoxicity. *Biochem. Biophys. Res. Commun.* **285,** 217–223 CrossRef Medline
31. Gao, X., Lee, K., Reid, M. A., Sanderson, S. M., Qiu, C., Li, S., Liu, J., and Locasale, J. W. (2018) Serine availability influences mitochondrial dynamics and function through lipid metabolism. *Cell Rep.* **22,** 3507–3520 CrossRef Medline
32. Koves, T. R., Ussher, J. R., Noland, R. C., Slentz, D., Mosedale, M., Ilkayeva, O., Bain, J., Stevens, R., Dyck, J. R., Newgard, C. B., Lopaschuk, G. D., and Muoio, D. M. (2008) Mitochondrial overload and incomplete fatty acid oxidation contribute to skeletal muscle insulin resistance. *Cell Metab.* **7,** 45–56 CrossRef Medline
33. Owen, M. R., Doran, E., and Halestrap, A. P. (2000) Evidence that metformin exerts its anti-diabetic effects through inhibition of complex 1 of the mitochondrial respiratory chain. *Biochem. J.* **348,** 607–614 CrossRef Medline
34. Israelsen, W. J., Dayton, T. L., Davidson, S. M., Fiske, B. P., Hosios, A. M., Bellinger, G., Li, J., Yu, Y., Sasaki, M., Horner, J. W., Burga, L. N., Xie, J., Jurczak, M. J., DePinho, R. A., Clish, C. B., *et al.* (2013) PKM2 isoform-specific deletion reveals a differential requirement for pyruvate kinase in tumor cells. *Cell* **155,** 397–409 CrossRef Medline
35. Christofk, H. R., Vander Heiden, M. G., Harris, M. H., Ramanathan, A., Gerszten, R. E., Wei, R., Fleming, M. D., Schreiber, S. L., and Cantley, L. C. (2008) The M2 splice isoform of pyruvate kinase is important for cancer metabolism and tumour growth. *Nature* **452,** 230–233 CrossRef Medline
36. Patra, K. C., Wang, Q., Bhaskar, P. T., Miller, L., Wang, Z., Wheaton, W., Chandel, N., Laakso, M., Muller, W. J., Allen, E. L., Jha, A. K., Smolen, G. A., Clasquin, M. F., Robey, B., and Hay, N. (2013) Hexokinase 2 is required for tumor initiation and maintenance and its systemic deletion is therapeutic in mouse models of cancer. *Cancer Cell* **24,** 213–228 CrossRef Medline
37. Faubert, B., Li, K. Y., Cai, L., Hensley, C. T., Kim, J., Zacharias, L. G., Yang, C., Do, Q. N., Doucette, S., Burguete, D., Li, H., Huet, G., Yuan, Q., Wigal, T., Butt, Y., *et al.* (2017) Lactate metabolism in human lung tumors. *Cell* **171,** 358–371.e9 CrossRef Medline
38. Madhukar, N. S., Warmoes, M. O., and Locasale, J. W. (2015) Organization of enzyme concentration across the metabolic network in cancer cells. *PLoS One* **10,** e0117131 CrossRef Medline
39. Pontén, F., Jirström, K., and Uhlén, M. (2008) The Human Protein Atlas—a tool for pathology. *J. Pathol.* **216,** 387–393 CrossRef Medline
40. Uhlén, M., Björling, E., Agaton, C., Szigyarto, C. A., Amini, B., Andersen, E., Andersson, A. C., Angelidou, P., Asplund, A., Asplund, C., Berglund, L., Bergström, K., Brumer, H., Cerjan, D., Ekström, M., *et al.* (2005) A human protein atlas for normal and cancer tissues based on antibody proteomics. *Mol. Cell. Proteomics* **4,** 1920–1932 CrossRef Medline
41. Pacella, I., Procaccini, C., Focaccetti, C., Miacci, S., Timperi, E., Faicchia, D., Severa, M., Rizzo, F., Coccia, E. M., Bonacina, F., Mitro, N., Norata, G. D., Rossetti, G., Ranzani, V., Pagani, M., *et al.* (2018) Fatty acid metabolism complements glycolysis in the selective regulatory T cell expansion during tumor growth. *Proc. Natl. Acad. Sci. U.S.A.* **115,** E6546–E6555 CrossRef Medline
42. Singleton, K. R., Crawford, L., Tsui, E., Manchester, H. E., Maertens, O., Liu, X., Liberti, M. V., Magpusao, A. N., Stein, E. M., Tingley, J. P., Frederick, D. T., Boland, G. M., Flaherty, K. T., McCall, S. J., Krepler, C., *et al.* (2017) Melanoma therapeutic strategies that select against resistance by exploiting MYC-driven evolutionary convergence. *Cell Rep.* **21,** 2796–2812 CrossRef Medline
43. Liu, X., Ser, Z., Cluntun, A. A., Mentch, S. J., and Locasale, J. W. (2014) A strategy for sensitive, large scale quantitative metabolomics. *J. Vis. Exp.* 10.3791/51358 CrossRef Medline
44. Liu, X., Ser, Z., and Locasale, J. W. (2014) Development and quantitative evaluation of a high-resolution metabolomics technology. *Anal Chem.* **86,** 2175–2184 CrossRef Medline

# Evolved resistance to partial GAPDH inhibition results in loss of the Warburg effect and in a different state of glycolysis

Maria V. Liberti, Annamarie E. Allen, Vijyendra Ramesh, Ziwei Dai, Katherine R. Singleton, Zufeng Guo, Jun O. Liu, Kris C. Wood and Jason W. Locasale

*J. Biol. Chem. 2020, 295:111-124.*
*doi: 10.1074/jbc.RA119.010903 originally published online November 20, 2019*